Feedback control of chaotic motions and unstable wave packets in a space-time-dependent system

He Kaifen[1] and Hu Gang[1,2]

[1] *China Center of Advanced Science and Technology (World Laboratory), 8730, Beijing 100080, China and Institute of Low Energy Nuclear Physics, Beijing Normal University, Beijing 100875, China**

[2] *Department of Physics, Beijing Normal University, Beijing 100875, China and Institute of Theoretical Physics, Academia Sinica, P. O. Box 2735, Beijing 100875, China*

(Received 16 February 1995; revised manuscript received 26 June 1995)

By using feedback control in k space and pinning in x space we successfully stabilize unstable steady wave-packet solutions in a representation of the driven/damped nonlinear drift-wave system. Three typical solutions are chosen to be controlled. Without controlling they display different dynamical features: one is chaotic in time while coherent in space, another is chaotic both in time and in space, the third one is explosively unstable. All the states can be stabilized to the respective unstable regular reference states by our controlling schemes.

PACS number(s): 05.45.+b, 03.40.Kf, 52.35.−g

I. INTRODUCTION

Chaotic and turbulent behaviors occur in a variety of nonlinear dynamic systems. In many cases such behaviors are considered to be harmful. For instance, in magnetically confined plasmas anomalous energy and particle transport across magnetic field can be induced by fully developed turbulence that causes undesirable energy loss. As well known, for chaotic systems a trajectory is very sensitive to perturbations; two orbits starting from neighboring points in phase space will separate exponentially from each other as time goes on. For this reason chaotic systems are generally accepted to be unpredictable and hardly controllable. However, it turns out in recent years that chaotic systems are not so difficult to control [1–12]. Different methods have been proposed to control chaos. For example, by Ott-Grebogi-York method [1] one can stabilize unstable periodic orbits embedded in a chaotic attractor. Feedback control [3,5] with respect to dynamic variables is also demonstrated to be very effective in suppressing chaos, and it is easy to realize in experiments. Most theoretical works on controlling chaos focus on systems described by ordinary differential equation's (ode's) or by low-dimensional mappings. Recently, however, there has appeared a great interest in controlling nonlinear extended systems [13–17]. In this paper we present, along the line of our previous Letter [13], an investigation on controlling spatiotemporal chaos. In Sec. II we specify our partial differential equation (pde) model and derive a set of mode equations for the perturbation to a steady wave from the model pde. The controlling schemes are described in Sec. III. In Sec. IV the results of the controlling are shown for three typical dynamically different states. In particular, we present an example of controlling a state that is chaotic both in time and in space. Since we will use truncated mode equations as the representation for the original pde, the meaning of "chaotic in time and space" will be restricted and explained later. Section V gives some discussions.

II. MODEL EQUATION

The following equation is taken as the system to be controlled [18],

$$\frac{\partial\phi}{\partial t}+a\frac{\partial^3\phi}{\partial t\partial x^2}+c\frac{\partial\phi}{\partial x}+f\phi\frac{\partial\phi}{\partial x}=-\gamma\phi-\epsilon\sin(x-\Omega t). \tag{1}$$

The equation with $\gamma=\epsilon=0$ is called nonlinear drift-wave equation [19] or regularized long-wave equation [20]. A periodic boundary condition $\phi(x+2\pi,t)=\phi(x,t)$ is used throughout the paper. This model is of importance in both fluid and plasma fields. If a nonuniform plasma is embedded in a magnetic field $\mathbf{B}=B\hat{\mathbf{z}}$, drift waves can be excited. The equation can be derived as follows [25]. The momentum equation of ions reads

$$\frac{d\mathbf{v}_i}{dt}=-\frac{e}{m_i}\nabla\Phi+\frac{eB}{m_iC}\mathbf{v}_{\perp i}\times\hat{\mathbf{z}}; \tag{2}$$

here and in the following the subscripts $\|$, $\perp$ indicate the directions of parallel and perpendicular to $\hat{\mathbf{z}}$, and the subscripts i,e the ion and electron, respectively. C is the light speed. Φ is a fluctuating electric potential. For drift-wave oscillations, the typical frequency $\omega\ll\Omega_i\equiv eB/m_iC$, and the parallel wavelength $2\pi/k_\|$ is in the order of the gradient scale length of the nonuniform plasma, which is much longer than the perpendicular wavelength $2\pi/k_\perp$. To the lowest-order approximation the left-hand side (lhs) of Eq. (2) can be neglected, one obtains the perpendicular velocity of the ions, $\mathbf{v}_{\perp i}=\mathbf{v}_E$, here

*Mailing address.

$$\mathbf{v}_E = \frac{C\hat{\mathbf{z}} \times \nabla_\perp \Phi}{B}. \tag{3}$$

For further approximation, we start from Eq. (2) in the perpendicular direction. Substituting $\mathbf{v}_{\perp i} = \mathbf{v}_E$ into its lhs, $d\mathbf{v}_{\perp i}/dt \equiv [\partial/\partial t + (\mathbf{v}_i \cdot \nabla)]\mathbf{v}_{\perp i}$, and neglecting the term with $\nabla_\parallel \sim k_\parallel$, one obtains $\mathbf{v}_{\perp i} = \mathbf{v}_E + \mathbf{v}_P$, here $\mathbf{v}_P$ is the polarization drift,

$$\mathbf{v}_P = -\frac{C}{B\Omega_i}\left(\frac{\partial}{\partial t} + \mathbf{v}_E \cdot \nabla_\perp\right)\nabla_\perp \Phi. \tag{4}$$

The continuity equation for ion is

$$\frac{\partial n_i}{\partial t} + \nabla \cdot (n_i \mathbf{v}_i) = 0, \tag{5}$$

where $\mathbf{v}_i = v_\parallel \hat{\mathbf{z}} + \mathbf{v}_{\perp i}$, and $\mathbf{v}_{\perp i} = \mathbf{v}_E + \mathbf{v}_P$. Now assume adiabatic electron density

$$n_e(\mathbf{r}, t) = n(x)\exp[e\Phi(\mathbf{r}, t)/T_e(x)];$$

here the mean density n and electron temperature T_e depend on the radial coordinate x only. With quasineutrality condition $n_i = n_e$ and confined to one-dimensional limit, one obtains, for $\phi = e\Phi/T_e$,

$$\left(1 - \rho_s^2 \frac{\partial^2}{\partial y^2}\right)\frac{\partial \phi}{\partial t} - \kappa_n c_s \rho_s \frac{\partial \phi}{\partial y} + \kappa_T c_s \rho_s \phi \frac{\partial \phi}{\partial y} = 0, \tag{6}$$

where $\kappa_n = (dn/dx)/n$, $\kappa_T = (dT_e/dx)/T_e$, $c_s = \sqrt{T_e/m_i}$, $\rho_s = c_s/\Omega_i$. Replacing y in Eq. (6) by x for the spatial coordinate, one obtains Eq. (1) with $\gamma = \epsilon = 0$. From the derivation we know that the coefficient a in Eq. (1) must be negative in physics. Here we fix $a = -0.287, c = 1.0, f = -6.0$ as we did in Ref. [18].

A sinusoidal wave $\epsilon \sin(x - \Omega t)$ is applied to Eq. (1) which, together with the damping term $-\gamma\phi$, can drive the system to a variety of different solutions, from stable steady wave packets up to turbulence. Different types of solutions can be distinguished, to a certain extent, by the "wave energy" $E(t)$ defined as

$$E(t) = \frac{1}{2\pi}\int_0^{2\pi} \frac{1}{2}[\phi^2(x,t) - a\phi_x^2(x,t)]dx. \tag{7}$$

Let us denote a steady wave packet solution of Eq. (1) as $\hat{\phi}(x - \Omega t)$, the corresponding wave energy $\hat{E}$ must be a constant (fixed point). $\hat{\phi}(x - \Omega t)$ can be stable or unstable. If $\hat{\phi}(x - \Omega t)$ is stable, $\hat{E}$ is a stable fixed point. Otherwise $\hat{E}$ is also unstable. In the simulations of Eq. (1) we have observed constant, periodic, quasiperiodic, chaotic $E(t)$.

A steady wave solution $\hat{\phi}(x - \Omega t)$ can be found algebraically if we transform the system to the reference frame following the driving wave $\sin(x - \Omega t)$. For this purpose let us set $\xi = x - \Omega t$; Eq. (1) then becomes

$$\frac{\partial}{\partial t}\left[\phi + a\frac{\partial^2 \phi}{\partial \xi^2}\right] - \Omega \frac{\partial}{\partial \xi}\left[\phi + a\frac{\partial^2 \phi}{\partial \xi^2}\right] + c\frac{\partial \phi}{\partial \xi} + f\phi\frac{\partial \phi}{\partial \xi} = -\gamma\phi - \epsilon \sin\xi. \tag{8}$$

A steady wave solution satisfies

$$-\Omega \frac{d}{d\xi}\left[\hat{\phi} + a\frac{d^2\hat{\phi}}{d\xi^2}\right] + c\frac{d\hat{\phi}}{d\xi} + f\hat{\phi}\frac{d\hat{\phi}}{d\xi} + \gamma\hat{\phi} + \epsilon\sin\xi = 0. \tag{9}$$

Substituting

$$\hat{\phi}(\xi) = \sum_{k=1}^{\infty} A_k \cos(k\xi + \theta_k) \tag{10}$$

into Eq. (9) one can solve the amplitude A_k's and phase θ_k's from the following set of equations:

$$-k[c - (1 - ak^2)\Omega]A_k \sin\theta_k + \gamma A_k \cos\theta_k - \frac{kf}{4}\left[\sum_{l+l'=k} A_l A_{l'} sin(\theta_l + \theta_{l'}) + \sum_{l-l'=k} A_l A_{l'} sin(\theta_l - \theta_{l'}) + \sum_{l'-l=k} A_l A_{l'} sin(\theta_{l'} - \theta_l)\right] = 0, \tag{11}$$

$$-k[c - (1 - ak^2)\Omega]A_k cos\theta_k - \gamma A_k sin\theta_k + \epsilon\delta_{1,k} - \frac{kf}{4}\left[\sum_{l+l'=k} A_l A_{l'} cos(\theta_l + \theta_{l'}) + \sum_{l-l'=k} A_l A_{l'} cos(\theta_l - \theta_{l'}) + \sum_{l'-l=k} A_l A_{l'} cos(\theta_{l'} - \theta_l)\right] = 0. \tag{12}$$

Here and in the following $k = 1, 2, \ldots, N(N \to \infty)$ and

$$\delta_{1,k} = \begin{cases} 1, & \text{if } k = 1; \\ 0, & \text{if } k \neq 1. \end{cases}$$

In a series of Ω regimes the dependence of the steady wave energy

$$\hat{E} = \sum_{k=1}^{\infty}(1 - ak^2)A_k^2/4 \tag{13}$$

on ϵ may form bistable curves. Figure 1 presents two groups of such S-shaped curves $\hat{E}(\epsilon)$, one in Fig. 1(a) is for $\Omega = 0.50 - 0.65$, the other in Fig. 1(b) for $\Omega = 0.285 - 0.34$.

In Sec. IV three typical solutions will be taken as our reference states for controlling, they are as follows. Case 1: $\Omega = 0.65, \epsilon = 0.20$; case 2: $\Omega = 0.34, \epsilon = 0.19$; and case 3: $\Omega = 0.56, \epsilon = 0.07$. The parameter conditions of these cases are marked in Figs. 1(a) and 1(b) by plusses. They locate either in the lower branches or in the middle branch of the S-shaped bistable curves $\hat{E}(\epsilon)$. At all these three parameter combinations the reference steady states are unstable. To describe their dynamics it is very convenient to use a set of equations for the modes of perturbation wave to the steady wave packets. First we divide the solution of Eq. (8) into two parts,

$$\phi(\xi,t) = \hat{\phi}(\xi) + \delta\phi(\xi,t); \tag{14}$$

here $\delta\phi$ is a deviation from the steady wave, which obeys the following equation:

$$\frac{\partial}{\partial t}\left[1 + a\frac{\partial^2}{\partial\xi^2}\right]\delta\phi - \Omega\frac{\partial}{\partial\xi}\left[1 + a\frac{\partial^2}{\partial\xi^2}\right]\delta\phi + c\frac{\partial\delta\phi}{\partial\xi} + f\frac{\partial}{\partial\xi}[\hat{\phi}(\xi)\delta\phi] + f\delta\phi\frac{\partial}{\partial\xi}\delta\phi = 0. \tag{15}$$

Substituting the Fourier expansions of $\hat{\phi}$, Eq. (10), and of $\delta\phi$,

$$\delta\phi(\xi,t) = \sum_{k=1}^{\infty} b_k(t)\cos[k\xi + \alpha_k(t)], \tag{16}$$

into Eq. (15), one can then obtain a set of equations for the deviation amplitudes and phases $\{b_k, \alpha_k\}$,

$$\dot{b}_k = N_k(t), \tag{17}$$

$$\dot{\alpha}_k = M_k(t), \tag{18}$$

where

$$N_k(t) = -\frac{\gamma}{1-ak^2}b_k + \frac{fk}{2(1-ak^2)}\left\{\sum_{l+l'=k}[A_l b_{l'}\sin(\theta_l + \alpha_{l'} - \alpha_k) + b_l b_{l'}\sin(\alpha_l + \alpha_{l'} - \alpha_k)] + \sum_{l-l'=k}[A_l b_{l'}\sin(\theta_l - \alpha_{l'} - \alpha_k) + b_l b_{l'}\sin(\alpha_l - \alpha_{l'} - \alpha_k)] + \sum_{l'-l=k}[A_l b_{l'}\sin(-\theta_l + \alpha_{l'} - \alpha_k) + b_l b_{l'}\sin(-\alpha_l + \alpha_{l'} - \alpha_k)]\right\}, \tag{19}$$

$$M_k(t) = -k\left[\frac{c}{1-ak^2} - \Omega\right] - \frac{fk}{2(1-ak^2)b_k}\left\{\sum_{l+l'=k}[A_l b_{l'}\cos(\theta_l + \alpha_{l'} - \alpha_k) + b_l b_{l'}\cos(\alpha_l + \alpha_{l'} - \alpha_k)] + \sum_{l-l'=k}[A_l b_{l'}\cos(\theta_l - \alpha_{l'} - \alpha_k) + b_l b_{l'}\cos(\alpha_l - \alpha_{l'} - \alpha_k)] + \sum_{l'-l=k}[A_l b_{l'}\cos(-\theta_l + \alpha_{l'} - \alpha_k) + b_l b_{l'}\cos(-\alpha_l + \alpha_{l'} - \alpha_k)]\right\}. \tag{20}$$

For Cases 1–3, the solutions of the mode Eqs. (17) and (18) with appropriate truncations agree with the direct numerical simulations of Eq. (1) [18,23].

In general for a system with $2N$-dimensional phase space, the phase volume element is $dV = \prod_{k=1}^{N} dq_k dp_k$; here q_k and p_k are the coordinates of phase space, respectively. The growth rate of phase volume can be obtained as

$$d\dot{V} = \Gamma dV = \sum_{k=1}^{N}\left(\frac{\partial\dot{q}_k}{\partial q_k} + \frac{\partial\dot{p}_k}{\partial p_k}\right)dV.$$

In representation Eqs. (17) and (18), the phase volume can be expressed as

$$dV = \prod_{k=1}^{N} b_k db_k d\alpha_k = \frac{1}{2}\prod_{k=1}^{N} db_k^2 d\alpha_k.$$

Then one has

$$\Gamma \equiv \frac{d\dot{V}}{dV} = \sum_{k=1}^{N}\left[\frac{\partial(\dot{b}_k^2)}{\partial(b_k^2)} + \frac{\partial\dot{\alpha}_k}{\partial\alpha_k}\right] = \sum_{k=1}^{N}\frac{1}{b_k}\frac{\partial}{\partial b_k}\left(b_k\frac{db_k}{dt}\right) + \sum_{k=1}^{N}\frac{\partial}{\partial\alpha_k}\left(\frac{d\alpha_k}{dt}\right) = -\sum_{k=1}^{N}\frac{2\gamma}{1-ak^2}. \tag{21}$$

The last equality can be obtained by using Eqs. (17) and (18); all the nonlinear terms are canceled with each other in the summations [24]. When $-\gamma < 0$ the phase volume contracts with constant rate $\sum_k 2\gamma/(1-ak^2)$.

With nonzero $\delta\phi(\xi,t)$, the wave energy deviates from the steady wave energy. The difference is

$$\delta E(t) = E(t) - \hat{E} \equiv \frac{1}{2}\sum_k (1-ak^2)A_k b_k(t)\cos[\theta_k - \alpha_k(t)] + \frac{1}{4}\sum_k (1-ak^2)b_k^2(t). \quad (22)$$

The first term in the right-hand side of Eq. (22) arises from the interaction between $\hat{\phi}(\xi)$ and $\delta\phi(\xi,t)$, the second one gives the self-energy of the deviation $\delta\phi$.

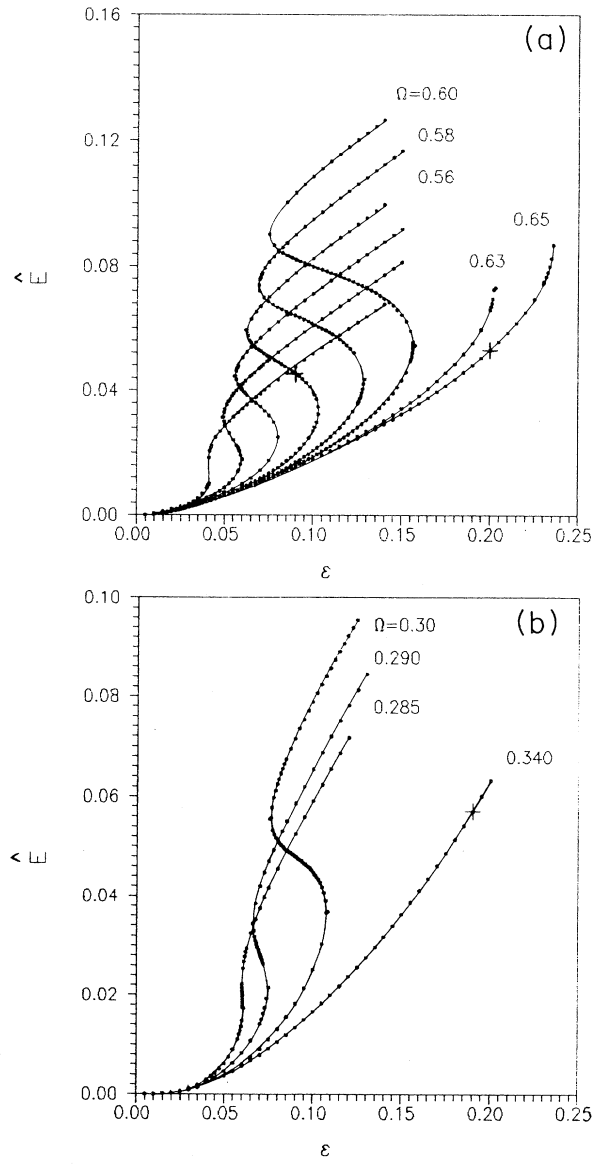

FIG. 1. Bistable steady wave energies $\hat{E}(\epsilon)$ in the regimes of (a) $\Omega = 0.50 - 0.65$ and (b) $\Omega = 0.285 - 0.34$. In the plots the + signs give the positions of cases 1, 2, and 3, respectively.

III. FEEDBACK CONTROL IN K SPACE AND IN X SPACE

A direct way to stabilize an unstable $\hat{\phi}(\xi)$ is to force Eq. (1) by a negative feedback $-\eta[\phi(\xi,t) - \hat{\phi}(\xi)]$. At a sufficiently large η a stabilization of the given reference state can be established for certainty. However, this feedback is difficult to realize practically since one has to monitor each point in x space (or each mode in k space) and respond to the system changes everywhere (or for every mode). There are two convenient ways to control the system:

The first is to monitor a single mode (e.g., $k = i$) and then input a monochromatic wave $-\eta b_i(t)$ to control the system. To this end Eq. (17) for $k = i$ is changed to

$$\dot{b}_{k=i} = N_i(t) - \eta b_i(t)/(1-ai^2), \quad (23)$$

and all the other equations for $b_{k\neq i}(t)$ and for $\alpha_k(t)$ remain the same as in Eqs. (17) and (18). With the feedback term the contracting rate of the phase volume becomes

$$\Gamma = -\sum_k \frac{2\gamma}{1-ak^2} - \frac{2\eta}{1-ai^2}. \quad (24)$$

The phase volume contracts faster when the feedback term with $-\eta < 0$ is applied.

The second scheme is to monitor a local region in x space and to apply feedback to the system in this region. A practical way may be to add a term such as $-(\eta/\pi r)[\phi(x,t) - \hat{\phi}(x-\Omega t)]\exp[-(x-x_0)^2/r], 0 \ll r \ll 1$; for numerical simplicity we can take the limit $r \to 0$ and use $-\eta\delta(x-x_0)[\phi(x,t) - \hat{\phi}(x-\Omega t)]$. In this case Eqs. (17) and (18) are replaced by

$$\dot{b}_k(t) = N_k(t) - \eta g_k(t), \quad (25)$$

$$\dot{\alpha}_k(t) = M_k(t) - \eta h_k(t), \quad (26)$$

with

$$g_k(t) = \frac{1}{1-ak^2}\sum_{l=1}^{\infty} b_l \cos[(l-k)(x_0 - \Omega t) + \alpha_l - \alpha_k],$$

$$h_k(t) = \frac{1}{1-ak^2}\sum_{l=1}^{\infty} b_l \sin[(l-k)(x_0 - \Omega t) + \alpha_l - \alpha_k]/b_k.$$

One can see that when pinning in x space, the feedback is applied practically to every Fourier mode of the system. Possibly this is why, as can be seen in the following, pinning in x space is very effective in our case.

When a pinning is applied, the additional contracting rate of the phase volume in Γ is no longer a constant. This is different from the controlling in k space. In the following we will see that when a chaotic state is controlled to the steady state by Eqs. (23), $\delta E(t)$ converges to zero practically monotonously after a short transient time (see Fig. 4), while for controlling by pinning [Eqs. (25) and (26)], $\delta E(t)$ makes excursions from time to time (see Fig. 8), although on the whole it ap-

proaches zero.

To perform a local controlling in x space, one can insert an electrode at a given point x_0 to monitor the variations of the system, and then change these measured data into electronic, magnetic or other signals, and use these signals as certain forces to drive the system to the aim state. This method can be conveniently applied in many practical systems. For k-space control one has to make a spatial Fourier transformation of the field, and work out variations of the desired harmonic waves. Thus, monitoring in k space must be more difficult than in x space in applications. However, this scheme can be also practical in certain special cases, for instance, in optical systems where different modes are separable in far field. One can conveniently monitor a single or a few modes and make feedback responses according to the measurements. Usually, the system relaxation time is much longer than the signal propagation time. Then one can regard the responses as instant feedbacks. In this case, as for response to the system, it is often sufficient to inject only one or few harmonic waves to control high-dimensional systems, which is very convenient in practice. In both methods when the aim state is finally approached the controlling term automatically goes to infinitely small as one expects for feedback control.

IV. NUMERICAL RESULTS OF CONTROLLING UNSTABLE WAVE PACKETS

By using the controlling methods in Sec. III, we have tried to control spatio-temporal chaos for many combinations of parameters with Ω ranging from 0.30 to 0.7. Both controlling schemes of Eq. (23) and Eqs. (25) and (26) work well. Here we focus on presenting the results of the three parameter combinations shown in Fig. 1, i.e., cases 1–3. All the reference states are unstable, and dynamically each of them has its own distinctive characteristics. In the calculations we use the truncation $N = 20$ for the mode equations of $\hat{\phi}$ as well as of $\delta\phi$. Truncation to how many modes depends on the parameter regimes, which may be relevant to the fact of which mode or modes plays a critical role in the instabilities of the steady wave solution. This matter will not be considered further. We only emphasize that a comparison of the solutions of truncated Eqs. (17) and (18) with the direct simulations [18,23] of Eq. (1) shows that our truncations are valid for cases 1–3; when increasing N no considerable change is found in the dynamics of the states.

A. Case 1

Without control the system is chaotic. Figure 2 shows (a) δE versus t, (b) the phase plot in the b_1-b_2 plane, and (c) $\phi(k)$, the spectrum of $\phi(x)$ in k space. It is found that for case 1 the motion is chaotic only in time; in space it still looks coherent. In Fig. 2(c) one can see that the strengths of the Fourier components in k space decrease exponentially with k when $k \geq 2$. This is very different from case 2 [see Fig. 9(c)], where the state has a wide spectrum in k space. In Fig. 3 we show the space-

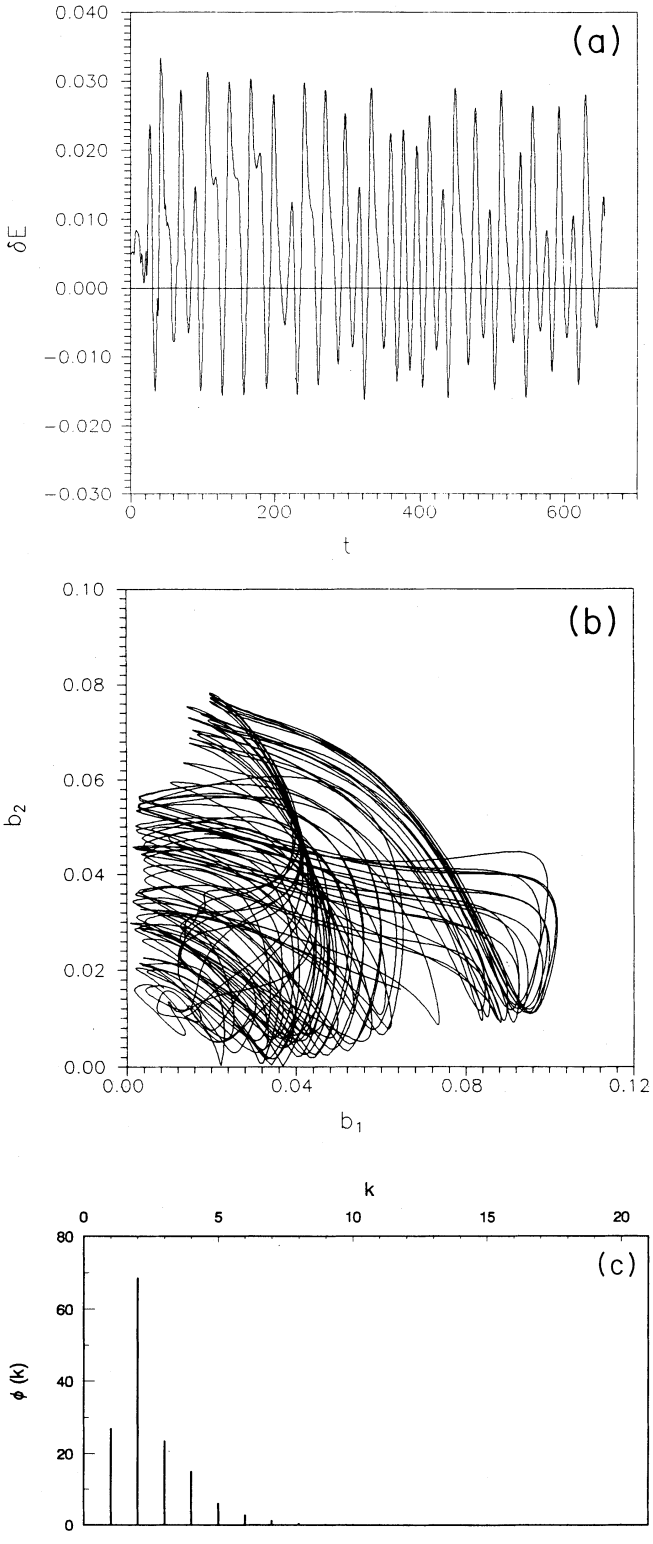

FIG. 2. Chaotic motions of case 1, $\Omega = 0.65, \epsilon = 0.20$, no control. The time evolutions of the perturbed energy δE and of the modes are chaotic, but the state is regular in space. (a) $\delta E(t)$, (b) $b_1(t)$ vs $b_2(t)$, (c) $\phi(k)$, the spectrum of $\phi(x)$ in k space. The amplitudes of the modes $k \geq 2$ decrease exponentially with k.

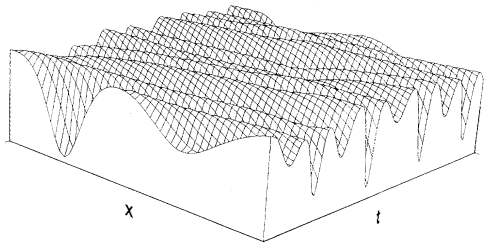

FIG. 3. Space-time dependence of $\phi(x,t)$ in case 1, $\Omega = 0.65, \epsilon = 0.20$, no control. One can see it is chaotic in time while coherent in space.

time dependence, $\phi(x,t)$, of case 1. One can see that the variation of ϕ in space is rather smooth. Nevertheless, $\phi(x,t)$ is not a steady wave, its spatial pattern varies irregularly with time, and the time evolutions of the mode amplitudes and phases as well as of the wave energy are chaotic.

The aim state ϕ can be controlled by injecting a monochromatic wave with $i = 1$ or $i = 2$. In Figs. 4(a) and 4(b) we plot $\delta E(t)$ and $b_2(t)$ for the case of injecting a monochromatic wave with $i = 2$ and $\eta = 1.0$. The projection of the trajectory in the b_1-b_2 plane is shown in Fig. 4(c). The aim state is approached after a certain transient time. It is remarkable that the chaotic motions of 40-dimensional systems ($N = 20$) can be controlled by feeding back only one equation. In Fig. 5 we plot $b_1(t)\cos[\alpha_1(t)]$ versus $b_2(t)\cos[\alpha_2(t)]$, the condition is the same as in Fig. 4, the transient states have been omitted. One can see that the orbit winds up smoothly to smaller and smaller cycles. The underlying mechanism is that the additional feeding term can create a potential well centered at $\delta\phi = 0$ to change the reference state from repelling to attracting so long as $\{i, \eta\}$ are properly chosen.

Investigation shows that when we suppress chaos of case 1 by injecting only one monochromatic wave of $i = 1$ (or 2), there exist both lower and upper thresholds for η, if $\eta_L < \eta < \eta_U$ the aim state can be reached. When $\eta < \eta_L$ the system can either be attracted to limit cycles or, if η is too small, remains chaotic. If $\eta > \eta_U$, though the chaotic motions can be suppressed the system cannot reach the aim state $\hat{\phi}$, instead it will asymptotically approach another steady state with nonzero δE. On the other hand, if we input two waves with $i = 1, 2$ simultaneously, there is only a lower threshold, the system can always be controlled to the aim state so long as $\eta > \eta_L$. Figure 6 plots the transient time T_c as a function of η; here T_c is determined by the condition that $|\delta E|$ keeps less than 10^{-4} in sufficiently long time (e.g., in 20 time steps, $\Delta t = 10^{-2}$). The signs "+" and "×" show the results of feedback with $i = 2$ and with both waves $i = 1, 2$, respectively. It is interesting to see from the plot that the variation of T_c with η shows stairs. In both cases one can find an optimum η at which the state can be controlled to steady state in the shortest time.

The system response to injecting monochromatic wave with $i \geq 3$ is different. In Fig. 7 we plot the trajectory in the b_1-b_2 plane obtained by injecting a monochromatic wave with $i = 3$ and $\eta = 1.0$. The transient process has been omitted. One can see that the system does

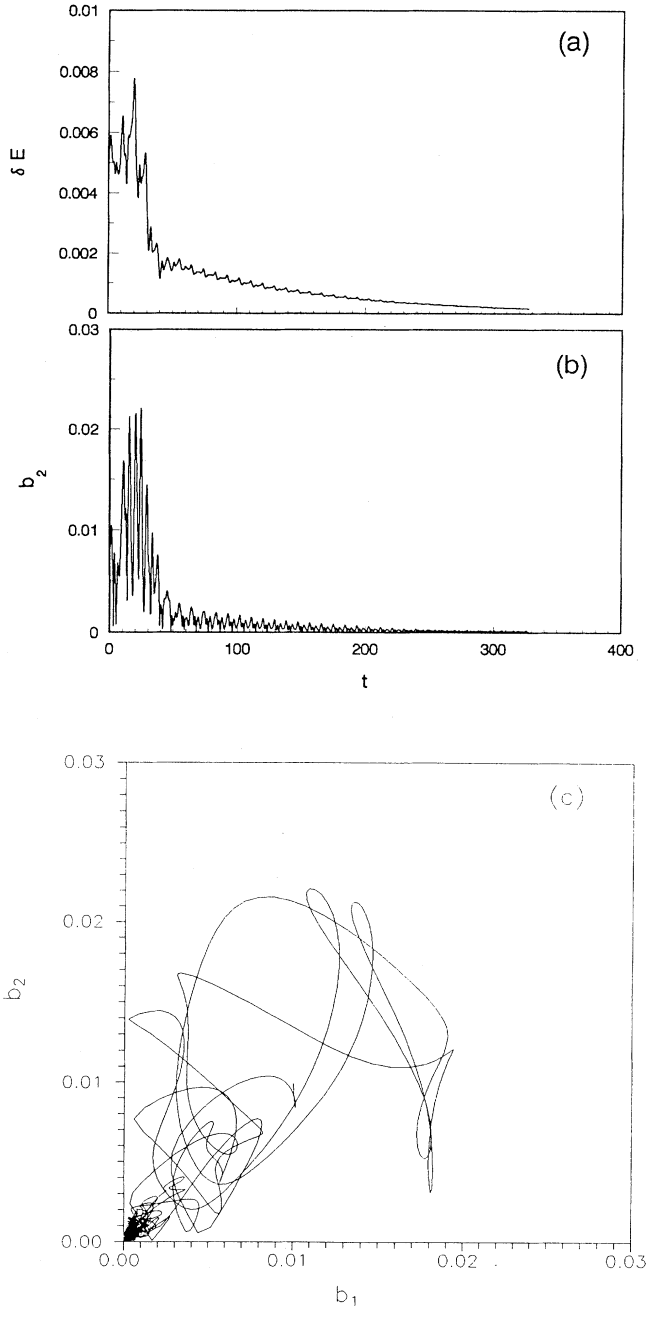

FIG. 4. Case 1 is controlled to the steady state by injecting a monochromatic wave $i = 2, \eta = 1.0$, (a) $\delta E(t)$, (b) $b_2(t)$, (c) $b_1(t)$ vs $b_2(t)$.

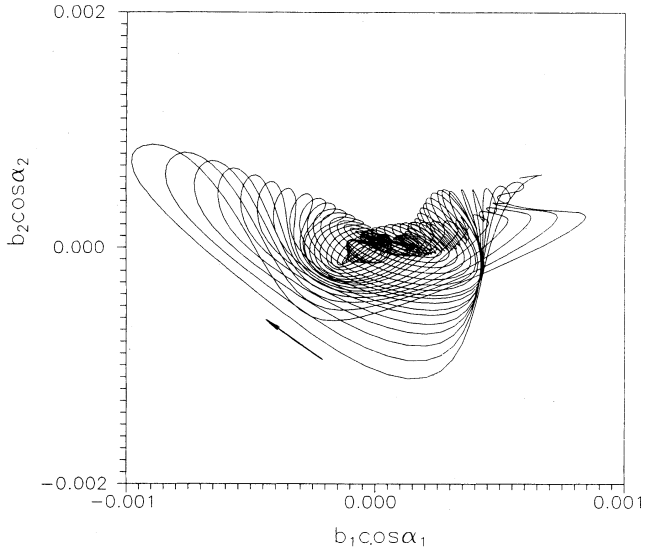

FIG. 5. $b_1(t)\cos\alpha_1(t)$ vs $b_2(t)\cos\alpha_2(t)$, the same condition as in Fig. 4, the arrow gives the direction of increasing time.

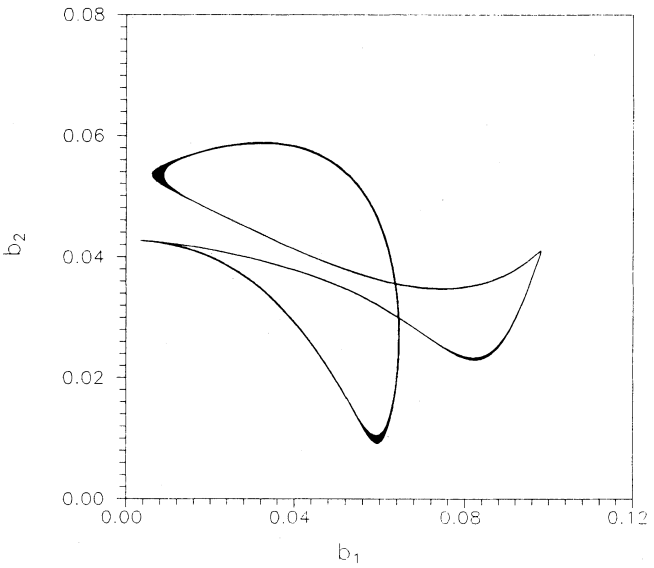

FIG. 7. When injecting a monochromatic wave $i = 3$, case 1 cannot be controlled to the aim state. This is an example controlled to a limit cycle when $\eta = 1.0$.

not approach the aim state $\hat{\phi}(\xi)$, instead it is attracted finally to a limit cycle. When η is increased to ~ 6.0 a steady state can be approached but δE is nonzero. We failed to control the system to $\hat{\phi}$ by injecting the wave with $i = 3$ at any η detected. Nevertheless, chaos can be successfully suppressed.

In Fig. 8 the results of pinning the state at $x_0 = 0$ with $\eta = 0.2$ are presented, where (a) δE versus t, (b) $\phi(0,t) - \hat{\phi}(x - \Omega t)|_{x=0}$ versus t. One can see that asymptotically the orbit converges to the steady state. In contrast to Fig. 4(a) of case 1 where δE approaches zero exponentially, in Fig. 8(a) after the transient time δE still makes excursions frequently for long times. This phenomenon can be explained by the time-dependent shrink-

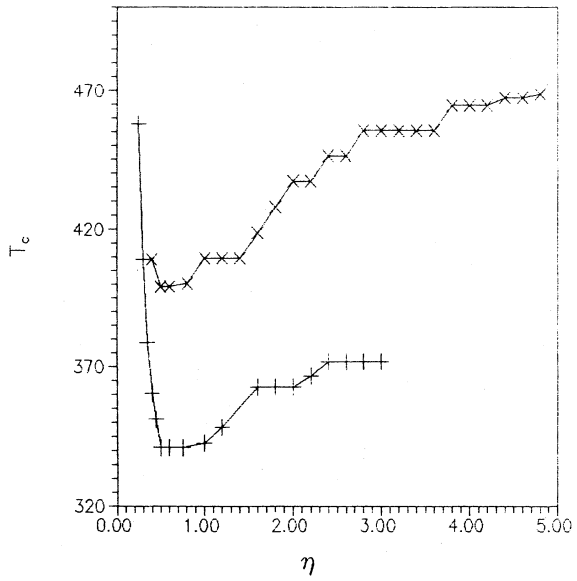

FIG. 6. Transient time T_c as a function of η; here T_c is recorded if δE remains less than 10^{-4} in subsequently 20 time steps $\Delta t(= 10^{-2})$, in the plot + gives a run of injecting one wave $i = 1$, $\times$ gives a run of injecting two waves $i = 1, 2$ (the same η values are used for $i = 1, 2$). One can see the stairs in T_c.

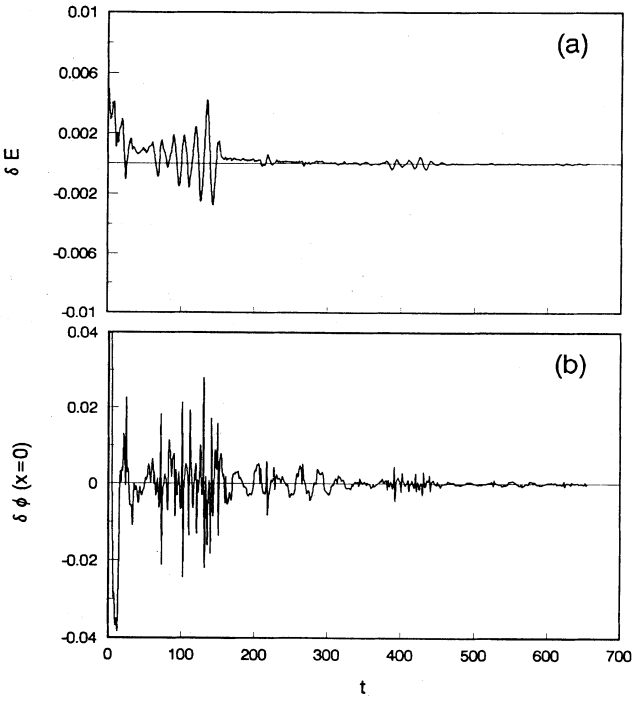

FIG. 8. Case 1 is controlled to the steady state by pinning at $x_0 = 0$ with $\eta = 0.2$. (a) δE vs t, (b) $\delta\phi$ vs t at $x = 0$.

ing rate of the phase volume of $\delta\phi$ as mentioned above. There is only a lower threshold η_L for pinning control; no upper threshold is found. Increasing η can shorten the transient time, however, a saturation relaxation time can be reached for very large η.

B. Case 2

Without control, the system state is also chaotic. However, the difference between case 1 and case 2 in dynamics is significant. In case 1 the spatial pattern of $\phi(x,t)$ is smooth, the chaos occurs only in its time evolution. But in Case 2 the motion of $\phi(x,t)$ is chaotic not only in time but also in space. Since we use truncation in the mode equations, we are actually dealing with a set of high- (but finite-) dimensional ordinary differential equations. Then the statement "chaotic in space" is not in the strict meaning. Here by chaotic in space we mean that the spatial variation recovered from the truncated modes looks rather random, and almost all the modes ranging to high k are excited. Figures 9(a) and 9(b) give δE versus t and $b_1(t)$ versus $b_2(t)$, respectively, both look more erratic than case 1 [Figs. 2(a) and 2(b)]. In Fig. 10 we plot $\phi(x,t)$ of case 2 vs both x and t, the field is no longer smooth and coherent in space. At any fixed time t, the spatial distribution $\phi(x)$ is irregular. $\phi(x)$ has a wide spectrum $\phi(k)$ in k space, and $\phi(k)$ varies dramatically with time. In Fig. 9(c) we give one example of $\phi(k)$. One can see that the amplitudes of all the 20 modes, including small k and large k, are manifesting in the spectrum, indicating that the modes with high k's are also very active in the motions. This is essentially distinguished from Fig. 2(c) of case 1 where the high k modes are quiescent; they are never excited when time goes on. It would be interesting whether our feedback scheme is still effective in such a turbulent case 2.

The spatial irregularity of case 2 is presumably caused by the overlap of the unstable regimes of different modes. This overlap can be observed by evaluating the nonlinear dependence of the mode eigenvalues on the parameters Ω and ϵ. The method is developed in Ref. [21,22]; here we simply give the result. In Figs. 11(a) and 11(b) for $\Omega = 0.34$ we plot the real and imaginary parts of the eigenvalues, $\lambda_{\tilde{k}}^{(r,i)}$ (the mode growth rate and eigenfrequency, $\tilde{k} = 1-5$), respectively versus ϵ. Here and in the following the subscript $\tilde{k}$ means that the eigenvalue (its real and/or imaginary parts) varies continuously from that of mode k at $\epsilon = 0$. When $\epsilon = 0$, $\hat{\phi}$ vanishes and one can get the exact eigenvalue $\lambda_k = -\gamma/(1-ak^2) + ik[c/(1-ak^2) - \Omega]$. With increasing ϵ, $\lambda_{\tilde{k}}$ changes nonlinearly with respect to ϵ due to the mode-mode couplings between the steady wave $\hat{\phi}$ and the deviation $\delta\phi$. From Fig. 11(b) one can see that in a certain range of ϵ the eigenfrequencies between modes $\tilde{k} = 1$ and 5 and between $\tilde{k} = 2$ and 3 are locked together, respectively, indicating the resonances of these two pairs of modes. As a result of the resonances $\lambda_{\tilde{k}=3}^{(r)}$ and $\lambda_{\tilde{k}=5}^{(r)}$ [the solid lines in Fig. 11(a)] cross zero, the two modes lose their stabilities. Their unstable regimes overlap with each other in the range of $0.18 < \epsilon < 0.25$.

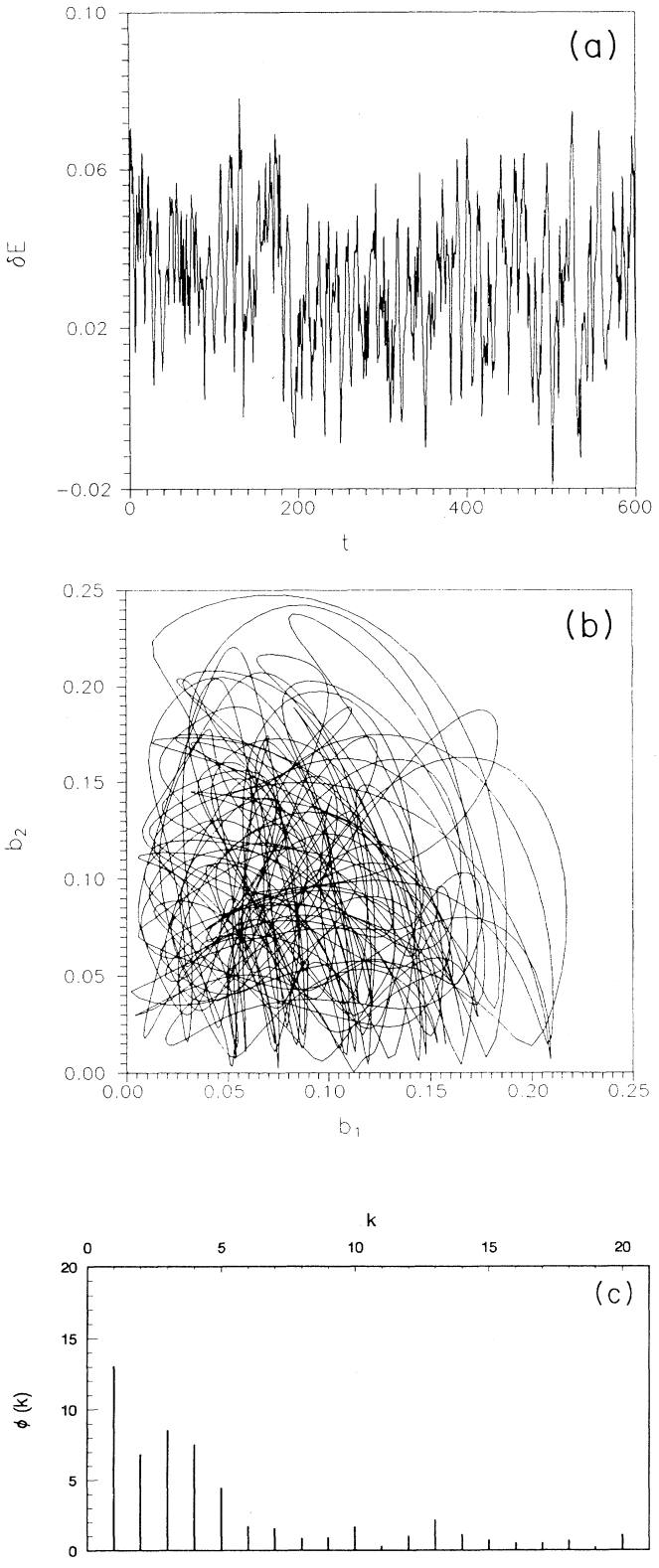

FIG. 9. Chaotic motions of case 2, $\Omega = 0.34, \epsilon = 0.19$, no control. (a) $\delta E(t)$; (b) $b_1(t)$ vs $b_2(t)$, the motions are very irregular compared with Fig. 2; and 2(c) $\phi(k)$, the spectrum of $\phi(x)$ in k space. The spectrum is wide, the high k modes are also manifesting.

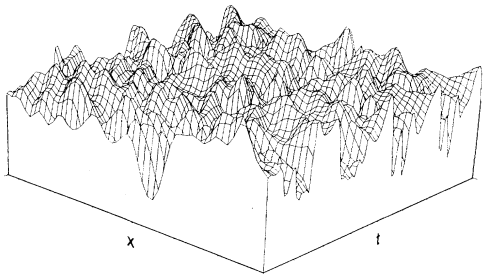

FIG. 10. Space-time dependence of $\phi(x,t)$ in case 2, $\Omega = 0.34, \epsilon = 0.19$, no control. It is chaotic in time as well as in space.

Case 2 ($\epsilon = 0.19$) is right in this range. No such overlap is found in case 1. This is probably the reason that the motions in case 2 lose spatial long range coherence but not in case 1.

It is striking that one can still suppress the space-time chaos of case 2 by injecting only one monochromatic

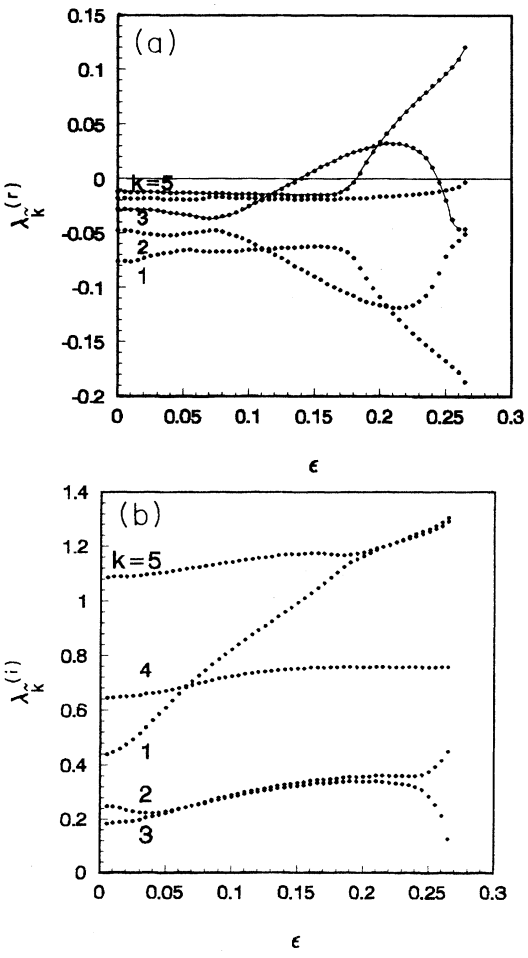

FIG. 11. The nonlinear variations of (a) real parts and (b) imaginary parts of eigenvalues $\lambda_{\tilde{k}}$ of mode $\tilde{k} = 1 - 5$ for $\Omega = 0.34$. In (a) the unstable regimes of mode $\tilde{k} = 3, 5$ (solid lines) overlap with each other in the range $\sim 0.18 < \epsilon < \sim 0.25$.

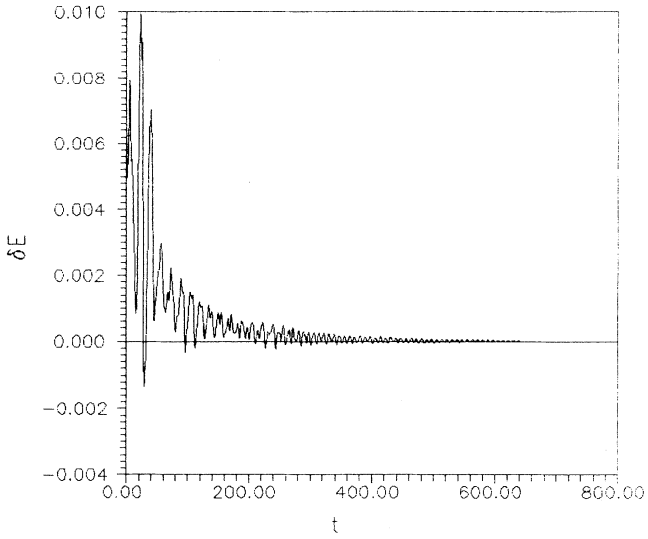

FIG. 12. Case 2 is controlled to the steady state by injecting a monochromatic wave of $i = 1$, $\eta = 1.0$. δE vs t.

wave. Figure 12 gives an example in which by injecting $i = 1, \eta = 1.0$ the aim state is arrived with $\delta E(t)$ going to zero.

Here we can discuss another interesting problem in k-space control, i.e., how to choose proper modes for controlling so that the number of feeding modes can be re-

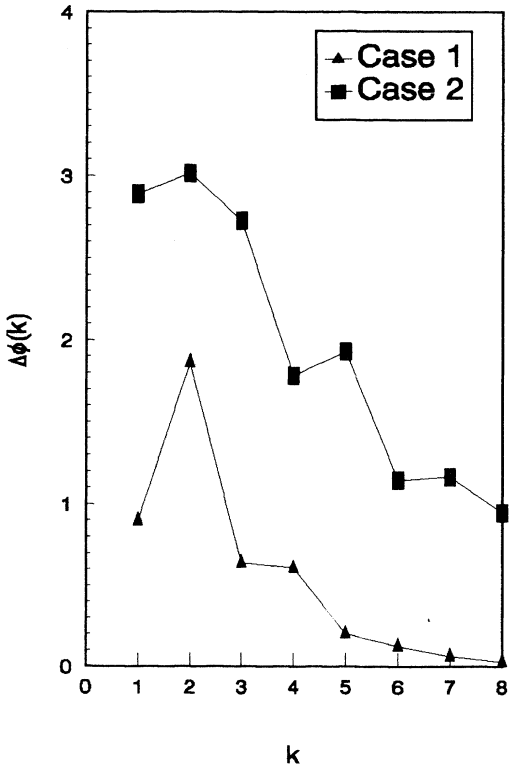

FIG. 13. $\Delta\phi(k)$, the mean square deviation of the amplitudes of Fourier components of $\phi(k)$ ($k = 1 - 8$) for case 1 and case 2.

duced to as few as possible. Our heuristic argument is based on the linear stability analysis of the unstable aim state. The efficiency may be good if we feed back the mode that has a small angle with respect to the most unstable manifold and has a large projection on it. In experiments and practical situations the above plausible argument may be of help to find proper modes for the k-space feedback control. For instance, from the linear stability analysis we know that in case 1 the nonlinear resonance between mode $\tilde{k} = 1, 2$ is responsible for the instability of the steady wave $\hat{\phi}$ (cf. Ref. [22]), in this case most probably mode 1 and 2 have smallest angles with respect to the unstable manifold. And indeed we successfully stabilize the unstable aim state by feeding back mode 1 or 2. As a comparison, we fail to stabilize the aim state by injecting mode $k = 3$ since this mode has a small projection on the unstable manifold. On the contrary, in case 2 we can successfully control the chaos by feeding back a single mode $k = 3$ (e.g., $i = 3, \eta = 2.0$)

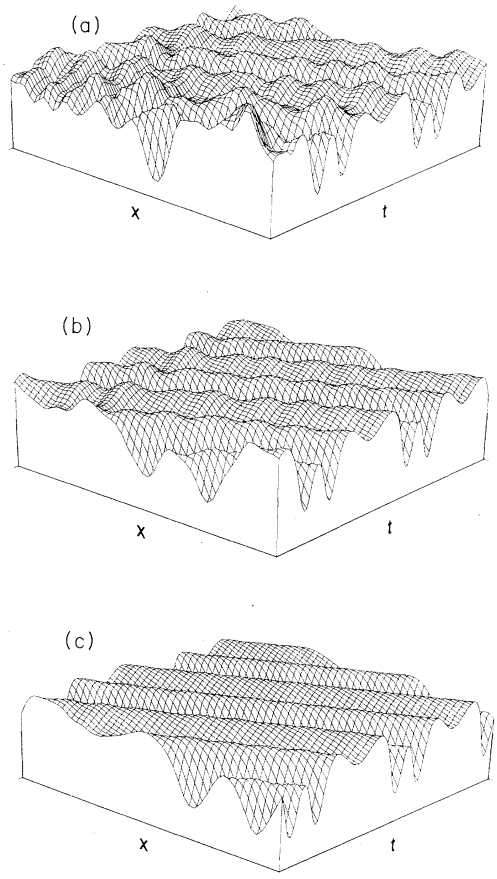

FIG. 14. The space-time dependence $\phi(x,t)$ of controlling case 2 by pinning at $x_0 = 0$ with $\eta = 1.0$. A wave packet of initially erratic both in time and in space is controlled finally to the steady wave. (a) $t = 0 - 40$, (b) $t = 40 - 80$, (c) $t = 80 - 120$.

despite the fact that the state is much more turbulent than that of case 1. The reason is that in case 2 the nonlinear resonance between modes $\tilde{k} = 3$ and $\tilde{k} = 2$ (cf. Fig. 11) is one of the causes for the instability of the steady wave, and so the Fourier mode $k = 3$ may have a small angle with respect to the most unstable manifold of the unstable aim state.

The information on the fluctuations in k spectra of $\phi(x,t)$ may also help us to choose the feeding modes in numerical or real experiments. For this purpose, first we work out $\phi(k, t_m)$ at a series of times $t_m (m = 1, 2, \ldots, M)$, and calculate the average value of $\phi(k)$

$$\bar{\phi}(k) = \frac{1}{M} \sum_{m=1}^{M} \phi(k, t_m),$$

the mean square deviation $\Delta\phi(k)$ can be obtained as

$$\Delta\phi(k) = \left\{ \sum_{m=1}^{M} [\phi(k, t_m) - \bar{\phi}(k)]^2 / (M-1) \right\}^{1/2}.$$

Among all the modes, one can choose those with larger $\Delta\phi(k)$ as the feeding modes. For example, one can see in Fig. 13 that for case 1 $\Delta\phi(k = 2)$ is the largest, while in our numerical tests $k = 2$ is the most effective feeding mode; and for case 2 $\Delta\phi(k)$ with $k = 1 - 3$ are the largest ones, as the feeding modes they are all effective for suppressing chaos.

Figure 14 gives an example of suppressing chaos by pinning the aim state at a fixed point $x_0 = 0, \eta = 1.0$. The calculation starts from a fully developed chaotic $\phi(x,t)$ state, which is realized after a sufficient long computing time without controlling. The controlling is added at $t = 0$. Figure 14 shows the space-time distributions $\phi(x,t)$, here

$$\phi(x,t) = \sum_{k=1}^{N} A_k \cos[k(x - \Omega t) + \theta_k] + \sum_{k=1}^{N} b_k(t) \cos[k(x - \Omega t) + \alpha_k(t)],$$

in which (a) $t = 0 - 40$, (b) $t = 40 - 80$, and (c) $t = 80 - 120$. One can see that at an early stage the pattern is very erratic in time and in space. As time goes on the regularity is gradually established by controlling. After about $t > 100$, complete regularity is realized and the solution becomes a traveling wave with constant amplitude and phase speed. As a comparison one can see that, in Fig. 10 when without controlling, the state starting from the same initial distribution $\phi(x, t = 0)$ as in Fig. 14 looks very turbulent.

C. Case 3

This is an explosively unstable state locating in the middle branch of the S-shaped $E(\epsilon)$ curve. If the state is disturbed the perturbation amplitude is unbounded unless it reaches another stable state. In this case we are

dealing with a wave packet in an unstable branch of a bistable curve rather than a chaotic state. The cause of the instability of the steady wave in case 3 is different from that in cases 1 and 2. For example, in Fig. 11, the unstable modes have complex conjugate eigenvalues, the instability of the steady wave packet is caused by the Hopf bifurcation. In case 3, however, the eigenfrequency of the unstable mode ($\tilde{k} = 2$ in this case) becomes zero, consequently the eigenvalues of $\tilde{k} = 2$ degenerate to a pair of real values (cf. [21,22]). From the physical point of view, it is very useful to suppress this unstable mode and make the middle branch stable by a very weak controlling. Without controlling, in order to drive the system from the lower (upper) branch to the upper (lower) branch one needs large perturbation to overcome the middle barrier. If the middle state is stabilized by a weak feedback one can rather flexibly realize the lower or upper state by taking off the feedback and switching on a small pushing up or down. The idea is realized in our case by using both Eqs. (23) and Eqs. (25) and (26). In Fig. 15(a) we plot δE versus t for $\Omega = 0.56$ and $\epsilon = 0.07$ without controlling, initially the state is very close to $\hat{\phi}$, it leaves the steady state exponentially with time. In Fig. 15(b) the state is controlled by using Eqs. (23) with $i = 2, \eta = 1.0$. The system is eventually locked to the middle branch, though the initial state is far from the aim state. We have tried other parameters, e.g., $i = 1, \eta = 1.0$ and $i = 3, \eta = 1.0$ the middle branch can always be stabilized. Pinning in x space is also effective to stabilize the middle branch.

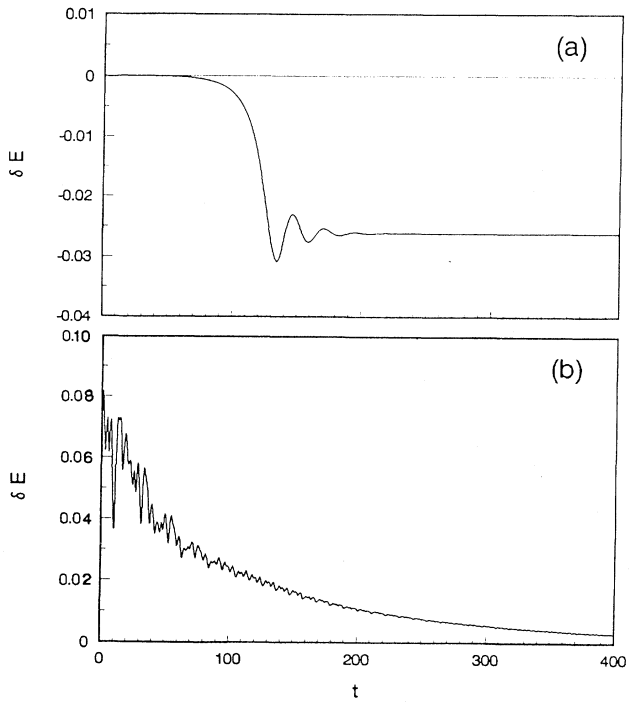

FIG. 15. Case 3 ($\Omega = 0.56, \epsilon = 0.07$) is stabilized by injecting a monochromatic wave $i = 2$, $\eta = 1.0$. (a) Without controlling, initially small δE deviates from zero exponentially with time. (b) Initial large δE goes to zero when injecting a monochromatic wave $i = 2$, $\eta = 1.0$.

V. DISCUSSION

In this paper we present in detail the numerical results of three special cases of controlling chaos in a space-time-dependent system. The k-space control and x-space pinning are found to be effective in suppressing spatiotemporal chaos rather generally. First, the approaches are not sensitive to the initial conditions. We have tried various distinct initial states (not too far from the aim state, otherwise it is possible that the system falls into a completely different basin), in all our three cases, spatiotemporal chaos can be successfully controlled. Second, the approaches work well in a wide range of parameter space, we have tested diverse parameter combinations in the range $0.3 < \Omega < 0.7$, the states are chosen in the lower or middle branches of the bistable curves (Fig. 1), the chaos can always be controlled by feeding back a single mode or pinning a single x point. In particular one can stabilize not only a state chaotic in time and regular in space but also a state chaotic both in time and in space. However, as we mentioned above, as a representation for a space-time-dependent system our model of mode equations is restricted, for further investigation one has to deal with the pde directly.

In general, the effectiveness of x-space pinning depends on the pinning location. Then it is an interesting problem in x-space control to choose proper space points through which injections can sensitively change the system dynamics and effectively drive the system toward the aim state. However, our model (1) has a symmetry invariant to the space displacement, and then the controlling efficiency does not depend on the choice of pinning point. It is remarkable that in our cases we are able to suppress chaos successfully by pinning only a single point. The reason might be that in our model the space correlation length is long. This long-range space correlation may be induced by the driving wave [the second term in the rhs of Eq. (1)]. In more general cases of space-time-dependent systems one has to inject more than one space point to control chaos. It is extremely important to estimate the lowest pinning density σ for a successful control. We guess that σ might be determined by the space correlation length L of the chaotic systems such that $1/\sigma \geq L$. However, this conjecture should be confirmed in future investigations on more space-time-dependent systems.

ACKNOWLEDGMENTS

This work is supported by National Natural Science Foundation of China, and National Basic Research Project "Nonlinear Science," and AAAPT.

[1] E. Ott, C. Grebogi, and J. A. York, Phys. Rev. Lett. **64**, 1196 (1990).
[2] W. L. Ditto, S. N. Rauseo, and M. L. Spano, Phys. Rev. Lett. **65**, 3211 (1990).
[3] E. R. Hunt, Phys. Rev. Lett. **66**, 1953 (1991).
[4] R. Roy, T. W. Murphy, T. D. Maier, Z. Gills, and E. R. Hunt, Phys. Rev. Lett. **68**, 1259 (1992).
[5] K. Pyragas, Phys. Lett. **170A**, 421 (1992).
[6] U. Dressier and G. Nitche, Phys. Rev. Lett. **68**, 1 (1992).
[7] R. Lima and M. Pettini, Phys. Rev. A **41**, 726 (1990).
[8] Y. Braiman and I. Goldhirst, Phys. Rev. Lett. **66**, 2545 (1991).
[9] P. Tham and A. K. Sen, Phys. Fluids B **4**, 3058 (1992).
[10] P. Tham and A. K. Sen, Phys. Rev. A **46**, 4520 (1992).
[11] J. A. Sepulchre and A. Babloyantz, Phys. Rev. E **48**, 954 (1993).
[12] G. Hu and Z. L. Qu, Phys. Rev. Lett. **72**, 68 (1994).
[13] G. Hu and K. F. He, Phys. Rev. Lett. **71**, 3794 (1993).
[14] D. Auerbach, Phys. Rev. Lett. **72**, 1184 (1994).
[15] F. Quin, E. E. Wolf, and H.-C. Chang, Phys. Rev. Lett. **72**, 1459 (1994).
[16] J. A. Sepulchre, I. Aranson, H. Levine, and L. Tsimring, Phys. Rev. Lett. **72**, 2561 (1993).
[17] G. A. Johnson, M. Löcher, and E. R. Hunt, Phys. Rev. E **51**, R1 (1995).
[18] K. F. He and A. Salat, Plasma Phys. Controlled Fusion **31**, 123 (1989).
[19] V. Oraevskii, H. Tasso, and H. Wobig, in *Plasma Physics and Controlled Nuclear Fusion Research*, Proceedings of the 3rd International Conference, Novosibirsk, 1968 (IAEA, Vienna 1969), Vol. I, p. 671.
[20] R. K. Dodd *et al.*, *Solitons and Nonlinear Wave Equation* (Academic, London, 1982), p. 596.
[21] K. F. He and G. Hu, Phys. Lett. **169A**, 341 (1992).
[22] K. F. He and G. Hu, Phys. Lett. **190A**, 38 (1994).
[23] A. Salat and K. F. He, Max-Planck Institute of Plasma Physics, Report No. IPP 6/280 (1989) (unpublished).
[24] Refer to, e.g., J. D. Meiss and W. Horton, Phys. Fluids **25**, 1838 (1982).
[25] Refer to W. Horton, Phys. Rep. **192**, 1 (1990).